

A motor neuron disease–associated mutation in p150^{Glued} perturbs dynactin function and induces protein aggregation

Jennifer R. Levy,¹ Charlotte J. Sumner,² Juliane P. Caviston,¹ Mariko K. Tokito,¹ Srikanth Ranganathan,² Lee A. Ligon,¹ Karen E. Wallace,¹ Bernadette H. LaMonte,¹ George G. Harmison,² Imke Puls,² Kenneth H. Fischbeck,² and Erika L.F. Holzbaur¹

¹Department of Physiology, School of Medicine, University of Pennsylvania, Philadelphia, PA 19104

²Neurogenetics Branch, National Institute of Neurological Disorders and Stroke, National Institutes of Health, Bethesda, MD 20892

The microtubule motor cytoplasmic dynein and its activator dynactin drive vesicular transport and mitotic spindle organization. Dynactin is ubiquitously expressed in eukaryotes, but a G59S mutation in the p150^{Glued} subunit of dynactin results in the specific degeneration of motor neurons. This mutation in the conserved cytoskeleton-associated protein, glycine-rich (CAP-Gly) domain lowers the affinity of p150^{Glued} for microtubules and EB1. Cell lines from patients are morphologically normal but show delayed recovery after nocodazole treat-

ment, consistent with a subtle disruption of dynein/dynactin function. The G59S mutation disrupts the folding of the CAP-Gly domain, resulting in aggregation of the p150^{Glued} protein both in vitro and in vivo, which is accompanied by an increase in cell death in a motor neuron cell line. Overexpression of the chaperone Hsp70 inhibits aggregate formation and prevents cell death. These data support a model in which a point mutation in p150^{Glued} causes both loss of dynein/dynactin function and gain of toxic function, which together lead to motor neuron cell death.

Introduction

The microtubule motor cytoplasmic dynein and its activator dynactin, which mediate minus end–directed movement, have important roles in both interphase and dividing cells. In interphase cells, the dynein–dynactin complex is essential for vesicle and organelle transport, such as ER-to-Golgi vesicular trafficking (for review see Schroer, 2004). The dynein–dynactin motor complex also transports RNA particles (Carson et al., 2001), aggresomes (Johnston et al., 2002), and virus particles along microtubules (Dohner et al., 2002). During cell division, dynein and dynactin play a critical role in both nuclear envelope breakdown and spindle formation (for review see Schroer, 2004).

Consistent with these multiple cellular roles, dynein and dynactin function are required in higher eukaryotes. Loss of dynein or dynactin is lethal in *Drosophila melanogaster*

(Gepner et al., 1996), and mice homozygous for loss of cytoplasmic dynein heavy chain die early in embryogenesis (Harada et al., 1998). Cells cultured from dynein heavy chain–null embryos show fragmented Golgi and a dispersal of endosomes and lysosomes throughout the cytoplasm (Harada et al., 1998).

Neurons appear to be particularly susceptible to defects in dynein–dynactin complex function. The dominant-negative mutation in *D. melanogaster* Glued, which encodes a truncated form of the p150^{Glued} subunit of dynactin, shows defects that are most profound in neurons (Harte and Kankel, 1983). Two *N*-ethyl-*N*-nitrosourea–induced point mutations in cytoplasmic dynein heavy chain cause slowly progressive motor neuron disease in mice (Hafezparast et al., 2003). *Legs at odd angles* (*Loa*) and *Cramping* (*Cra1*) mice each carry missense mutations in a highly conserved domain of cytoplasmic dynein that mediates subunit interactions. When homozygous, these mutations are lethal; heterozygous mice exhibit progressive loss of motor neurons, leading to muscle weakness and atrophy (Hafezparast et al., 2003). A similar phenotype is observed in transgenic mice with a targeted disruption of dynactin in motor neurons (LaMonte et al., 2002).

J.R. Levy and C.J. Sumner contributed equally to this paper.

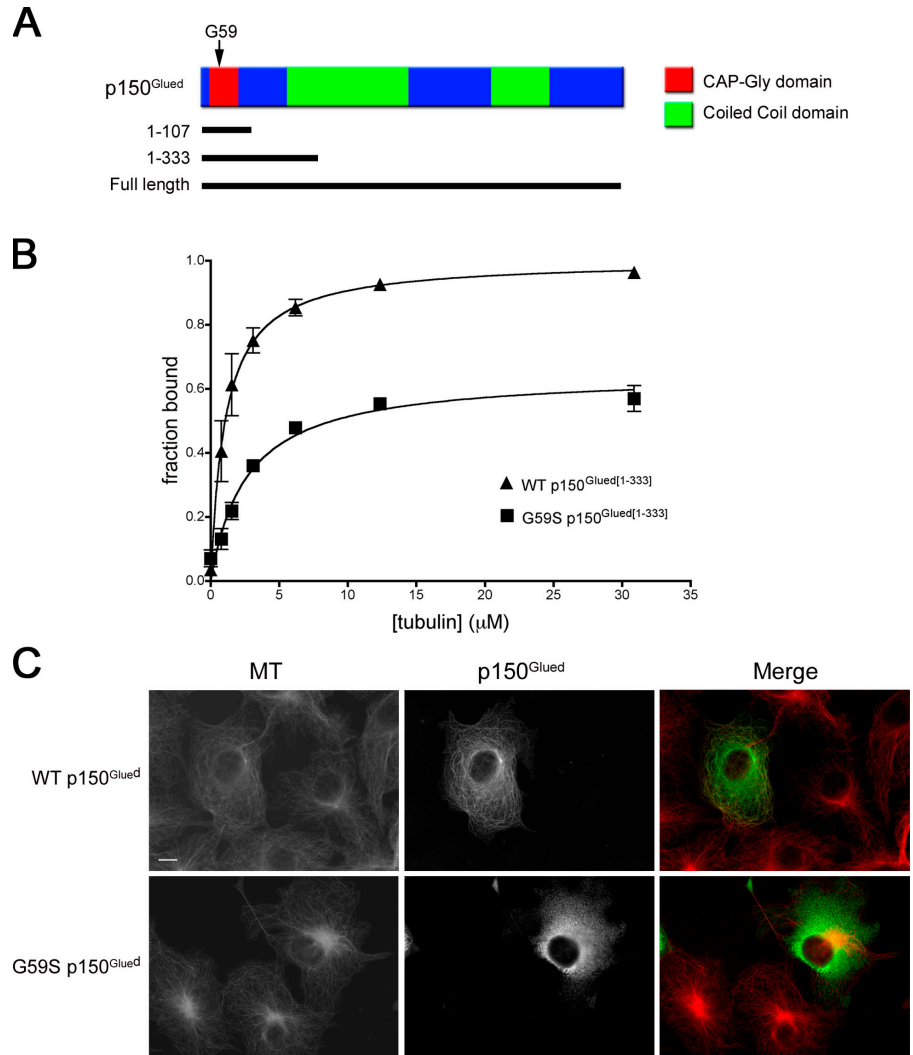
Correspondence to Erika L.F. Holzbaur: holzbaur@mail.med.upenn.edu

Abbreviations used in this paper: CAP-Gly, cytoskeleton-associated protein, glycine-rich; DIC, dynein intermediate chain; PI, propidium iodide; SOD1, superoxide dismutase.

The online version of this article contains supplemental material.

Figure 1. The G59S mutation impairs the binding of p150^{Glued} to microtubules.

(A) Schematic representation of p150^{Glued}. Glycine 59 lies in the CAP-Gly microtubule binding domain. The 1–107 fragment contains the CAP-Gly domain, and the 1–333 fragment contains the CAP-Gly domain, an adjacent serine-rich domain (residues 111–191), and a small part of the first predicted coiled-coil domain. (B) Wild-type (WT) and G59S p150^{Glued} were expressed in vitro and incubated with increasing concentrations of microtubules. The microtubule bound and unbound proteins were separated by centrifugation and visualized by SDS-PAGE and fluorography. The fraction bound, as determined by densitometry, was plotted against the concentration of tubulin \pm SEM and fitted to a rectangular hyperbola. (C) COS7 cells were transfected with GFP-tagged wild-type (top) or G59S (bottom) p150^{Glued}. Cells were fixed after 48 h and stained for GFP (green) and microtubules (red). Bar, 10 μ m.



In humans, a G59S missense mutation has been identified in the gene encoding p150^{Glued} (DCTN1) in a kindred with slowly progressive motor neuron disease (Puls et al., 2003). Affected patients develop adult-onset vocal fold paralysis, facial weakness, and distal-limb muscle weakness and atrophy. Clinical, electrophysiological, and pathological investigations have confirmed the selective loss of motor neurons in this disorder (Puls et al., 2005). p150^{Glued} is the dynein subunit responsible for binding to dynein and microtubules (Vaughan and Vallee, 1995; Waterman-Storer et al., 1995). The G59S substitution occurs in the highly conserved NH₂-terminal cytoskeleton-associated protein, glycine-rich (CAP-Gly) domain, which interacts directly with microtubules (Waterman-Storer et al., 1995) and the microtubule plus-end protein EB1 (Ligon et al., 2003).

In this study, we examined the biochemical and cellular effects of the G59S substitution in p150^{Glued}. Our data suggest that the G59S mutation leads to both decreased microtubule binding and enhanced dynein and dynactin aggregation, suggesting that both loss of function and toxic gain of function contribute to the motor neuron degeneration observed in affected patients.

Results

The G59S mutation disrupts the binding of p150^{Glued} to microtubules and EB1

The G59S mutation is located within the highly conserved CAP-Gly domain of the p150^{Glued} polypeptide, a domain that mediates the binding of dynactin to microtubules. We compared the microtubule binding affinities of wild-type and G59S p150^{Glued} peptides (Fig. 1 A). The CAP-Gly domain of wild-type p150^{Glued}, which spans residues 1–107, bound weakly to microtubules (unpublished data). This 1–107 peptide lacks the serine-rich region of p150^{Glued} (111–191), which may be required for efficient microtubule binding by CAP-Gly proteins (Hoogenraad et al., 2000). In contrast, the binding of NH₂-terminal residues 1–333 of the wild-type protein to microtubules was robust, with a K_d of $1.1 \pm 0.2 \mu$ M. The 1–333 fragment of p150^{Glued} carrying the G59S mutation bound to microtubules with a K_d of $2.6 \pm 0.5 \mu$ M, indicating a modest decrease in affinity. More striking, however, was the observation that even at saturating microtubule concentrations, only half of the mutant protein was able to bind to microtubules in this assay (Fig. 1 B). Similar results were observed in experiments with full-length wild-type and G59S p150^{Glued} (unpublished data).

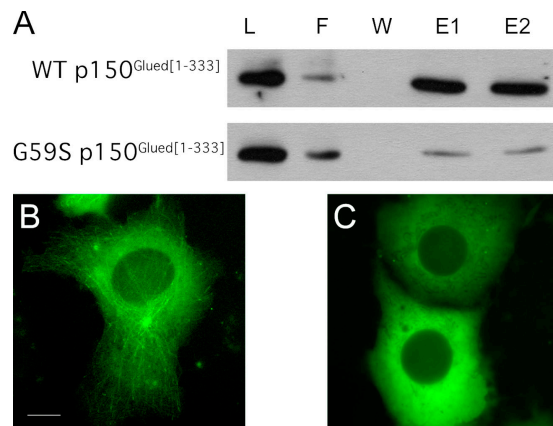


Figure 2. The G59S mutation impairs the binding of p150^{Glued} to EB1 and to microtubule plus ends. (A) Affinity chromatography of in vitro-translated wild-type (WT) or G59S p150^{Glued} (residues 1–333) over an EB1 column. Load (L), flow-through (F), wash (W), and eluate fractions (E1 and E2) were analyzed by SDS-PAGE and Western blot using a polyclonal antibody to p150^{Glued}. There is less G59S p150^{Glued} in the eluate fractions, in comparison to wild-type p150^{Glued}, indicating a decrease in G59S p150^{Glued} affinity for EB1. (B and C) Live cell fluorescence microscopy was used to observe the dynamics and localization of p150^{Glued} in COS7 cells expressing low levels of GFP-tagged wild-type (B) and G59S (C) p150^{Glued}. Bar, 10 μ m. B and C show still images from Videos 1 and 2, respectively [available at <http://www.jcb.org/cgi/content/full/jcb.200511068/DC1>].

We performed sequential microtubule binding experiments, in which the unbound fraction of G59S p150^{Glued} (1–333) protein was incubated for a second time with a saturating concentration of microtubules (25 μ M), and observed that ~60% of the protein pelleted with microtubules (Fig. S1 A, available at <http://www.jcb.org/cgi/content/full/jcb.200511068/DC1>). These data suggest that there may be a rapid equilibrium between two populations of the mutant polypeptide, one that can bind and one that cannot. Mixing of wild-type and G59S p150^{Glued} at a 1:1 ratio resulted in 60% of protein pelleting with 25 μ M microtubules (Fig. S1 B). These data suggest that mutant protein does not significantly inhibit the binding of wild-type polypeptide to microtubules.

We next investigated the effects of the mutation on the binding of p150^{Glued} to microtubules in cells. We used transient transfection assays to compare the distribution of wild-type and G59S p150^{Glued} in COS7 cells as well as MN1 cells, motor neuron-like cells that extend neurites (Salazar-Gruesso et al., 1991; Brooks et al., 1998). Although endogenous dynactin generally has a punctate cellular localization, with decoration of dynamic microtubule plus ends, overexpression of p150^{Glued} results in the decoration of the microtubule cytoskeleton (Waterman-Storer et al., 1995). As shown in Fig. 1 C, 24–48 h after transfection of GFP-tagged full-length constructs of wild-type p150^{Glued}, there was decoration of microtubules, as assessed by colocalization with tubulin. In contrast, GFP-tagged full-length G59S p150^{Glued} was distributed diffusely in the cytoplasm and showed no colocalization with tubulin (Fig. 1 C). Similar results were obtained using GFP-tagged NH₂-terminal 1–333 constructs of wild-type and G59S p150^{Glued},

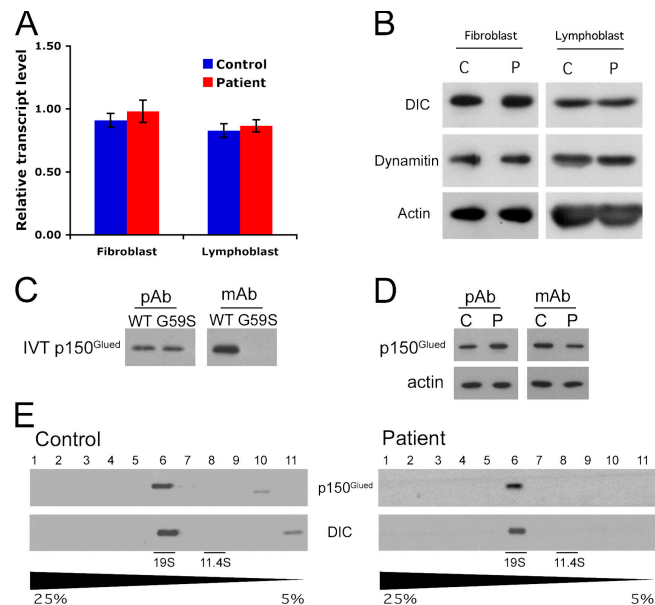


Figure 3. Expression of G59S p150^{Glued} does not alter the integrity of the dynactin complex. (A) Quantification of levels of p150^{Glued} RNA in lymphoblast and fibroblast cell lines derived from patients carrying the G59S mutation and unaffected controls, as measured by RT-PCR. $n = 3$. (B) Western blot analysis of dynactin expression levels in fibroblast and lymphoblast cell lines from control individuals (C) and patients heterozygous for the G59S mutation (P). Cell extracts were resolved by SDS-PAGE and probed for the dynactin subunit dynamitin, as well as DIC and actin. (C, right) An anti-p150^{Glued} monoclonal antibody (mAb) directed against the CAP-Gly domain does not recognize in vitro-translated (IVT) G59S p150^{Glued}. (left) An anti-p150^{Glued} polyclonal antibody (pAb) recognizes both the wild-type and mutant in vitro-translated protein. (D) Relative levels of total and wild-type p150^{Glued} expressed in fibroblasts isolated from patients carrying the G59S mutation. (E) Protein extracts from G59S and control fibroblast cell lines were sedimented on 5–25% sucrose gradients. The fractions were resolved by SDS-PAGE, and Western blot was performed using antibodies for the dynactin subunits p150^{Glued} and DIC. There is no peak of dynactin subunits in the lower density fractions, indicating that these subunits are incorporated into the dynactin complex.

as well as untagged full-length wild-type and G59S p150^{Glued} constructs (unpublished data). We performed microtubule binding experiments using protein extract from COS7 cells that had been transfected with GFP-tagged, full-length p150^{Glued}. Almost all of the exogenous polypeptide from wild-type p150^{Glued}-transfected cells pelleted with taxol-stabilized microtubules. However, only approximately half of the protein from G59S p150^{Glued}-transfected cells pelleted with microtubules (unpublished data). This observation confirms our in vitro data that only a portion of the G59S p150^{Glued} protein population may be available for microtubule binding.

The NH₂-terminal CAP-Gly domain of p150^{Glued} binds to EB1 (Ligon et al., 2003). Crystallographic studies demonstrate that the COOH terminus of EB1 contacts p150^{Glued} in a hydrophobic cleft of the CAP-Gly domain (Hayashi et al., 2005). We therefore examined the binding of G59S p150^{Glued} to EB1 using affinity chromatography. The wild-type peptide bound to the EB1 column and was retained until elution with high ionic strength buffer, but the G59S peptide had decreased retention on the column, indicating reduced affinity for EB1 (Fig. 2 A).

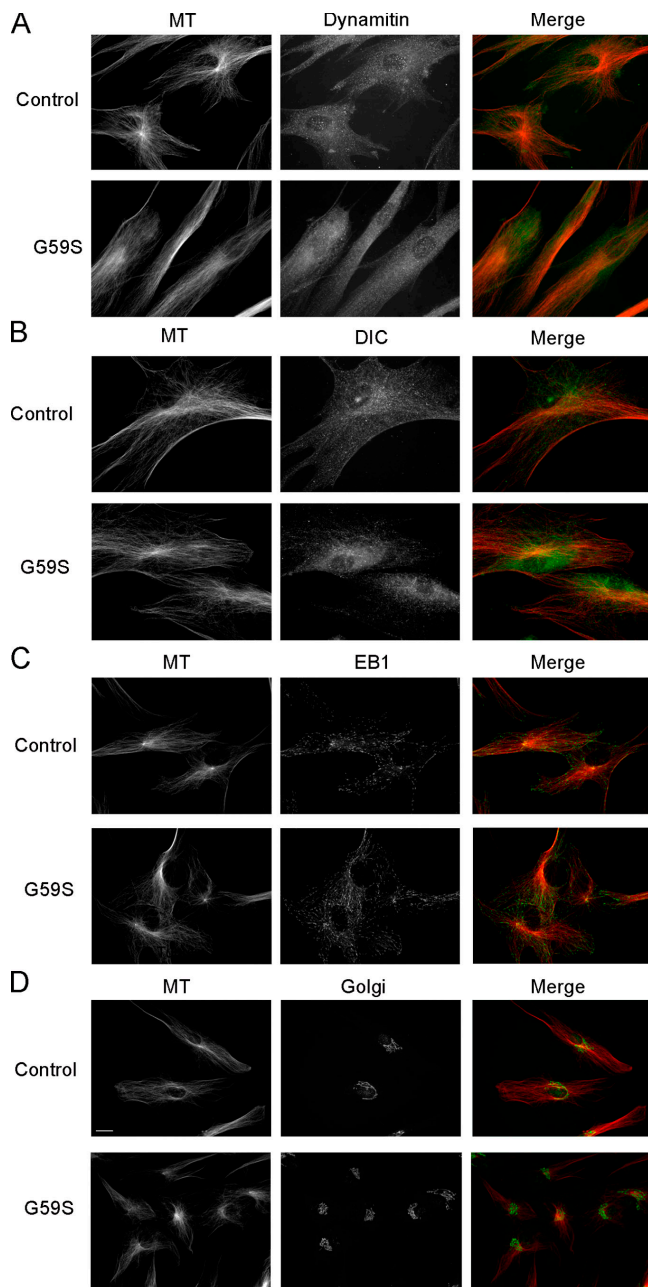


Figure 4. Dynein, dynactin, and EB1 are localized normally in cells heterozygous for the G59S mutation in p150^{Glued}. Control fibroblasts and fibroblasts from patients heterozygous for the G59S mutation were stained with antibodies to tubulin (MT; red) and dynamin (A), DIC (B), EB1 (C), and the Golgi marker GM130 (D). We observed no difference in morphology or microtubule organization in control and patient cells. There was a punctate, cytoplasmic localization of dynein and dynactin and microtubule tip localization of EB1 in both control and patient cells. The Golgi is intact and perinuclear in control and patient cells. Bar, 10 μ m.

Previous studies have shown that p150^{Glued} tracks dynamically with growing microtubule ends together with EB1 (Vaughan et al., 1999). To investigate the effect of the G59S mutation on the localization of p150^{Glued} to microtubule plus ends, we transfected COS7 cells with GFP-labeled wild-type or G59S p150^{Glued}. We selected for cells with low levels of expression, as microtubule plus-end tracking behavior is not

evident at higher expression levels because of the decoration and bundling of microtubules induced by high levels of exogenous p150^{Glued}. Wild-type p150^{Glued} tracked dynamically with growing microtubule ends (Fig. 2 B and Video 1, available at <http://www.jcb.org/cgi/content/full/jcb.200511068/DC1>), whereas the G59S construct showed no microtubule association, even at tips (Fig. 2 C and Video 2). In cells with higher levels of expression of the G59S construct, we noted apparent aggregates of misfolded protein, but these aggregates showed no directed movement (Video 2).

The G59S mutation does not alter the structural integrity of the dynactin complex

To study the cellular effects of the G59S mutation in the p150^{Glued} subunit of dynactin, we established fibroblast and lymphoblast cell lines from two symptomatic individuals known to be heterozygous for the G59S missense allele. Control fibroblast cell lines were obtained from two age-matched control individuals, and a control lymphoblast cell line was derived from an age-matched subject.

In these lines, we examined whether the G59S mutation alters the expression of dynein and dynactin. In both lymphoblasts and fibroblasts, quantitative RT-PCR analysis of RNA levels showed no difference in p150^{Glued} transcript levels between cell lines heterozygous for the G59S mutation and control cell lines (Fig. 3 A). Western blots of protein extract from patient cell lines showed up-regulation of levels p150^{Glued}, but not of dynein or other dynactin subunits, compared with control cell lines (Fig. 3, B and D).

To determine whether the wild-type and mutant proteins are both expressed in cells cultured from patients heterozygous for the G59S mutation, we performed quantitative Western blotting using both a monoclonal antibody to the microtubule binding region of p150^{Glued}, which binds the wild-type protein with a much higher affinity than the mutant protein, and a polyclonal antibody to p150^{Glued}, which recognizes both forms equally well (Fig. 3 C). Analysis of patient cells indicated that the total level of p150^{Glued} expression (as determined using the polyclonal antibody) is $147 \pm 7\%$ the level observed in control cells (Fig. 3 D). Western blots with the monoclonal antibody demonstrated that patient cells express $82 \pm 4\%$ of the wild-type p150^{Glued} that control cells express (Fig. 3 D). Thus, we estimate that the mutant protein makes up $\sim 44\%$ of the total p150^{Glued} population in patient cells.

To examine the structural integrity of the dynactin complex, we fractionated cell extracts from the patient-derived and control fibroblast cell lines by sucrose density gradient centrifugation. Intact dynactin was observed to sediment at $\sim 19S$ in both the patient and control samples, consistent with the large size of the multimeric complex. No significant pool of unincorporated p150^{Glued} subunits was observed in the lower S value fractions from either the patient or control cells (Fig. 3 E), suggesting that expression of the mutant polypeptide does not significantly disrupt dynactin structure and that the mutant polypeptide is incorporated into dynactin in these cells.

The heterozygous G59S mutation in p150^{Glued} does not disrupt dynein/dynactin localization, Golgi morphology, microtubule organization, or spindle assembly

Incorporation of the mutant polypeptide into dynactin might be expected to disrupt dynactin localization in patient-derived cells; however, we observed no change in the cellular localization of dynactin in fibroblasts derived from patients compared with control fibroblasts (Fig. 4 A and Fig. S2 A, available at <http://www.jcb.org/cgi/content/full/jcb.200511068/DC1>). Dynactin was present diffusely in the cytoplasm in a fine, punctate pattern, with no visible dynactin aggregates. We also noted no change in the cellular localization of cytoplasmic dynein, which was also found in a punctate cellular distribution, partially overlapping with dynactin staining in both patient and control cells (Fig. 4 B), or EB1, which was localized specifically to microtubule tips (Fig. 4 C).

We examined the effects of the G59S mutation on the integrity of the Golgi and the assembly of the mitotic spindle in the patient-derived fibroblasts. Disruption of dynactin by dynactin overexpression has been shown to disrupt the Golgi in interphase cells (Burkhardt et al., 1997) and the mitotic spindle in dividing cells (Echeverri et al., 1996). However, no gross morphological defects in the organization of the Golgi or the mitotic spindle were evident in patient-derived heterozygous cells under normal growth conditions (Fig. 4 D and Fig. S2 B). In addition, no consistent defects in the growth rate were observed in the patient fibroblasts (unpublished data).

The G59S mutation in p150^{Glued} impairs dynactin function

To test the patient fibroblasts for dynactin function, we looked at several dynein/dynactin-dependent processes. Dynactin, as well as dynein and the dynein-interacting protein LIS1, are necessary for directed fibroblast migration (Dujardin et al., 2003). However, wounded monolayers of patient cells recovered at the same rate as control cells (unpublished data). Aggresome formation has also been shown to be dynein dependent (Johnston et al., 2002). To test the effect of the mutation on aggresome formation, an androgen receptor containing an expanded polyglutamine repeat that induces inclusion formation (Merry et al., 1998) was expressed in patient fibroblasts. These fibroblasts formed inclusions at a rate indistinguishable from control cells (unpublished data).

Although a single wild-type copy of the gene for p150^{Glued} may be sufficient to mediate dynein-dependent processes under normal conditions, conditions of cellular stress may reveal latent effects of the G59S mutation. Nocodazole, a microtubule-depolymerizing drug, causes dispersal of the Golgi. During recovery from nocodazole treatment, microtubules reassemble and the Golgi fragments coalesce near the centrosome in a dynein/dynactin-dependent manner (Corthesy-Theulaz et al., 1992). Hafezparast et al. (2003) have shown a slowing in the recovery of the Golgi after nocodazole treatment in fibroblasts cultured from homozygous *Loa* mice. Therefore, we assayed the cytoskeletal and organelle recovery rates in heterozygous G59S and control fibroblasts after nocodazole washout.

Microtubules were depolymerized and the Golgi body dispersed after 1 h of nocodazole treatment. 1 h after drug washout, microtubules had reassembled in both control and patient-derived cells; however, Golgi complex morphology was significantly different in patient cells. In control cells, $75 \pm 2\%$ of cells had an intact Golgi complex, $22 \pm 3\%$ of cells had a partially disrupted Golgi complex, and $3 \pm 1\%$ of cells had completely disrupted Golgi complex (Fig. 5, A and B). In contrast, in patient-derived cells only $46 \pm 8\%$ of cells had intact Golgi complexes, whereas $44 \pm 5\%$ of cells showed partial disruption and $11 \pm 6\%$ of cells showed complete disruption of the Golgi. Golgi reassembly after 24 h was essentially normal in patient-derived fibroblasts (unpublished data), indicating that expression of mutant dynactin slows but does not block the minus end-directed transport of Golgi elements toward the microtubule organizing center.

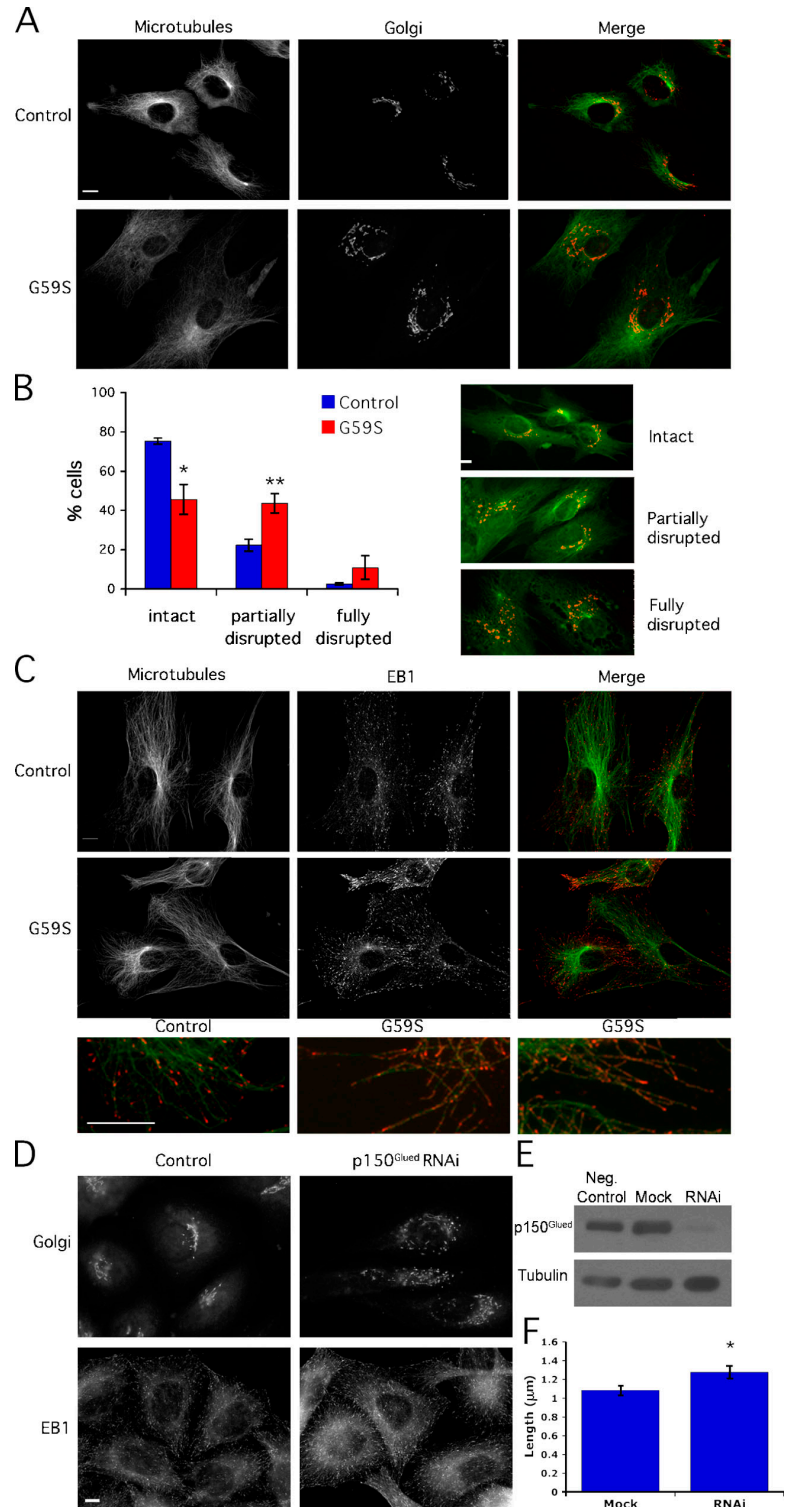
We also observed that the localization of EB1 to microtubule plus-end tips was altered in patient cells during nocodazole recovery. After microtubule depolymerization with nocodazole, EB1 demonstrated diffuse cytoplasmic staining. After 30 min of recovery in conditioned growth media, EB1 was localized specifically to the plus ends of microtubules in control cells, forming comet tails that were $1.20 \pm 0.06 \mu\text{m}$ long (Fig. 5 C). In patient-derived cells, EB1 was not limited to microtubule tips but was also observed to localize along microtubules (Fig. 5 C). EB1 tail length increased significantly in patient-derived cells, often to $>5 \mu\text{m}$, although overlap of adjacent microtubules prevented exact measurements of the elongated EB1 tails. These data suggest a defect in the specific localization of EB1 to microtubule plus ends.

To compare these data to a loss of function of dynactin, we used RNA interference to knockdown p150^{Glued} expression levels in HeLa cells by 70–90% (Fig. 5 E). This knockdown caused dispersal of the Golgi throughout the cell body (Fig. 5 D). In addition, we observed an increase in the length of EB1 comet tails from $1.08 \pm 0.05 \mu\text{m}$ in mock-transfected cells to $1.28 \pm 0.07 \mu\text{m}$ in cells transfected with small interfering RNA (Fig. 5 F). The lengthening of EB1 comet tails is similar to what was observed in patient fibroblasts recovering from nocodazole treatment and correlates with a loss of dynactin function.

The G59S mutation leads to aberrant aggregation of p150^{Glued}

In the microtubule binding assays described in Fig. 1, we observed the binding of only half of the mutant p150^{Glued} polypeptide to microtubules, suggesting that some portion of the mutant protein population is unavailable for binding to microtubules. To investigate this further, we expressed differentially tagged (T7 and His) truncated forms of wild-type and G59S p150^{Glued} in vitro and performed immunoprecipitation with an antibody to the T7 tag. Although our constructs, which include amino acids 1–333, span part of the first coiled-coil domain of p150^{Glued} hypothesized to mediate dimerization (Schroer, 2004), we observed no association of the T7- and His-tagged wild-type polypeptides (Fig. 6 A). However, we did observe coimmunoprecipitation of the differentially tagged NH₂-terminal G59S constructs. These data suggest that the G59S polypeptide, but not the wild type,

Figure 5. Cells heterozygous for the G59S mutation in p150^{Glued} have delayed recovery after microtubule depolymerization. Nocodazole washout experiments were performed on patient and control fibroblasts. Cells were treated with nocodazole for 1 h, washed twice with PBS, and returned to normal growth media. (A) After 1 h of recovery, cells were fixed and stained for the cis-Golgi marker GM130 (red) and microtubules (green). Control cells have compact and perinuclear Golgi, but patient cells have partially disrupted Golgi at the same time point after drug washout. (B) Quantification of Golgi morphology after 1 h of recovery, \pm SD (*, $P < 0.05$; **, $P < 0.01$). $n = 3$. (C) After 30 min of recovery, cells were fixed and stained for EB1 (red) and microtubules (green). Enlargements of merged images are shown at the bottom. Control cells show distinct tip localization of EB1, but patient cells show subtle mislocalization of EB1 along microtubules. (D) HeLa-M cells, either mock-transfected or transfected with small interfering RNA against p150^{Glued}, stained with antibodies for EB1 or trans-Golgi marker 46. (E) Knockdown of p150^{Glued}, compared with cells transfected with a fluorescein-labeled, nontargeting oligo or mock-transfected cells. (F) Quantification of the length of EB1 tails, \pm SD (*, $P < 0.05$). Bars, 10 μ m.



has a tendency to self-associate. There was no coimmunoprecipitation after incubation of differentially tagged wild-type and G59S p150^{Glued} (unpublished data), indicating that the wild-type and G59S proteins do not interact under these conditions.

We next investigated whether aberrant biochemical species of the G59S p150^{Glued} protein could be isolated from protein extracts of cells overexpressing this protein. COS7 cells were transfected with full-length wild-type or G59S GFP-tagged

p150^{Glued}. 24 h after transfection, the extract from these cells was fractionated over a sucrose gradient and analyzed by SDS-PAGE gel electrophoresis and Western blot. In cells transfected with wild-type p150^{Glued}, the peak concentration of dynamin and endogenous p150^{Glued} was at 19S (Fig. 6 B). The exogenous p150^{Glued} protein (as determined by the increase in molecular weight that is due to the GFP tag) was present at 19S, as well as at less dense fractions. This indicates that some exogenous

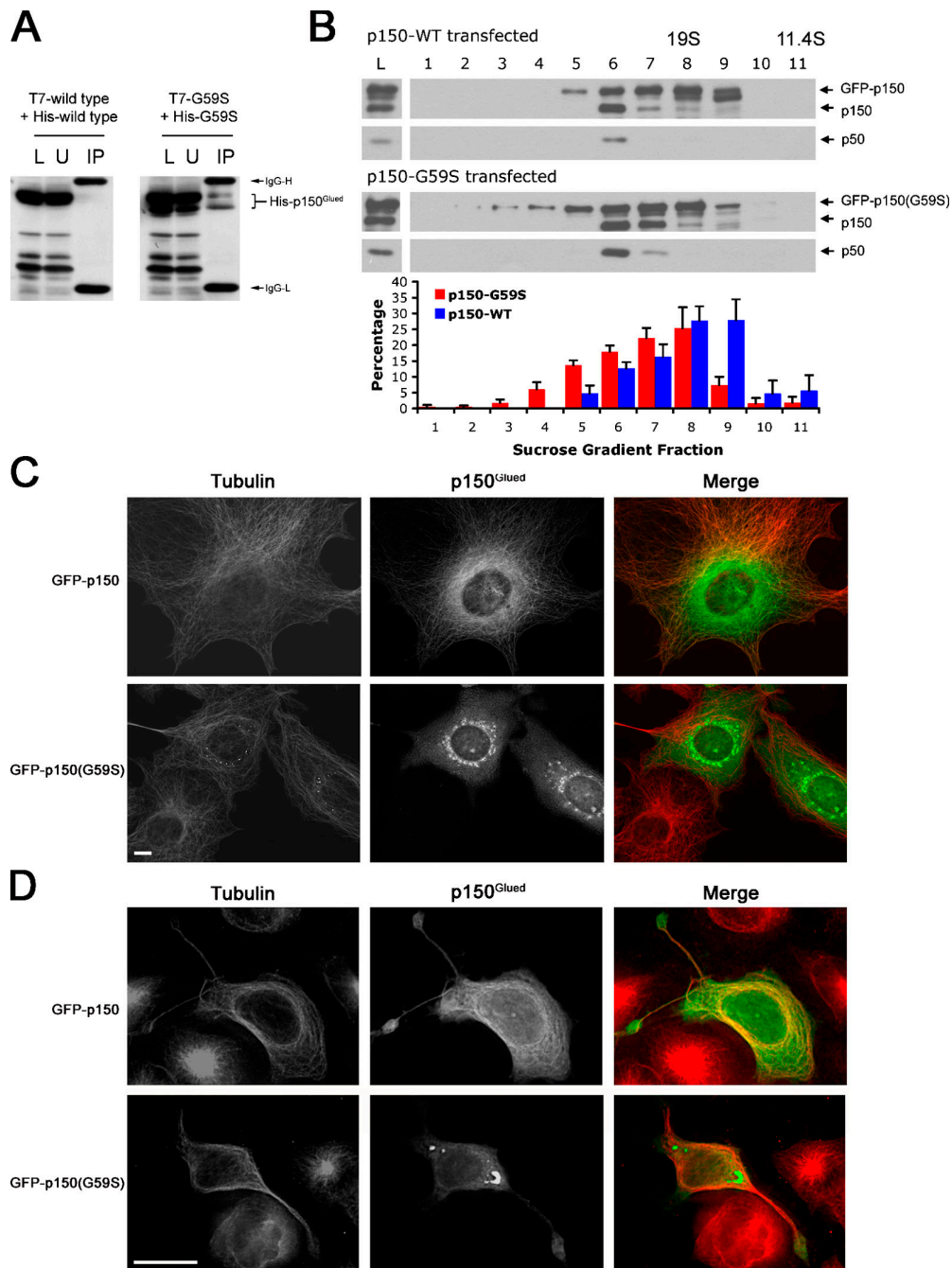
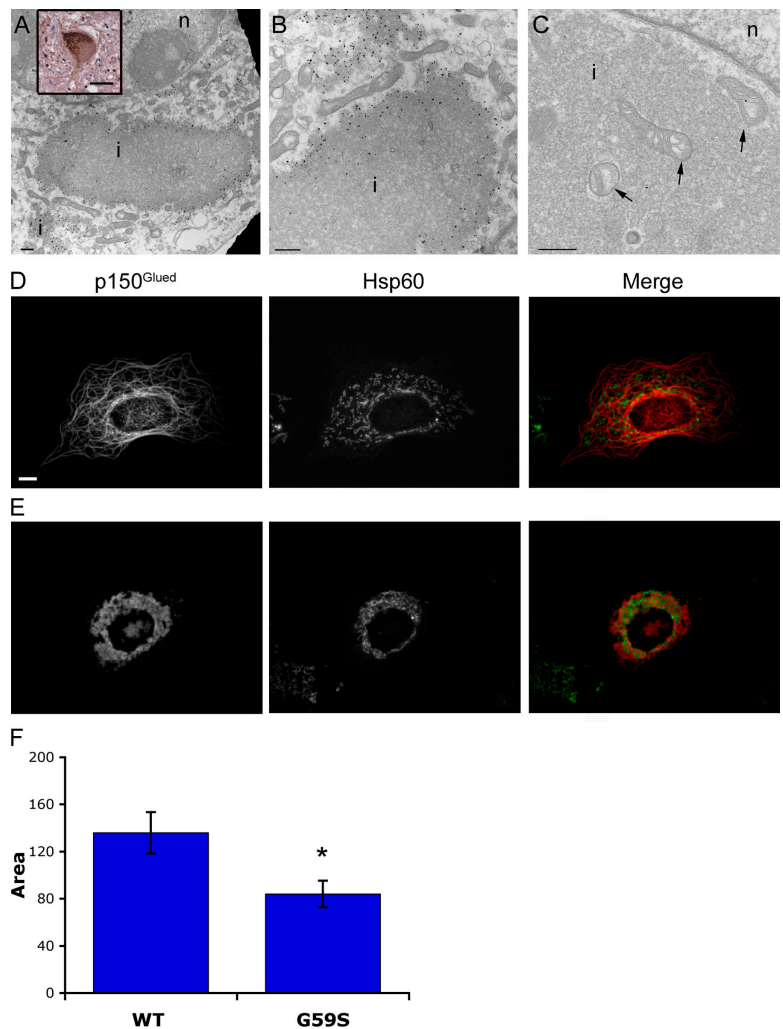


Figure 6. G59S p150^{Glued} aggregates in vitro and in vivo. (A) His- and T7-tagged constructs of wild-type and G59S p150^{Glued} were coexpressed in vitro. Immunoprecipitations were performed with anti-T7 antibody. The load (L), unbound (U), and immunoprecipitated (IP) fractions were resolved by SDS-PAGE and probed with antibodies to the His tag. The G59S construct, though not the wild type, runs as a doublet. We observed coimmunoprecipitation of the differentially tagged G59S constructs, indicating that the mutant protein self-associates. (B) Lysates from COS7 cells transfected with either GFP-tagged wild-type (WT) or G59S p150^{Glued} constructs were sedimented on 5–25% sucrose gradients. The fractions were resolved by SDS-PAGE and probed for the dynactin subunits p150^{Glued} and p50. The histogram indicates the mean percentage of protein in each fraction, as determined in three experiments, \pm SEM. G59S p150^{Glued} appears in the high-density fractions at a higher frequency than wild-type p150^{Glued}, which indicates it is incorporated into a high-molecular weight complex. $n = 4$. (C) COS7 cells transfected with GFP-tagged wild-type or G59S p150^{Glued} and fixed after 96 h. Bar, 10 μ m. (D) MN1 cells transfected with wild-type or G59S p150^{Glued}. Bar, 25 μ m.

protein is incorporated into the dynactin complex but some remains unincorporated in lower molecular weight fractions, most likely because its expression is in excess of the other subunits of dynactin. In contrast, extracts from cells transfected with GFP-tagged G59S p150^{Glued} demonstrated higher molecular weight species in fractions 2–4. This suggests the presence of

aggregated forms of G59S p150^{Glued} with a molecular weight well above that of endogenous dynactin (Fig. 6 B). Endogenous p150^{Glued} and dynamitin are not present in these fractions, indicating that they do not copurify with the aggregated protein. The aggregated protein remains soluble, as we did not observe the formation of detergent-insoluble aggregates (unpublished data).

Figure 7. The p150^{Glued} inclusions are associated with mitochondria. (A and B) Low-magnification (A) and high-magnification (B) electron micrographs of MN1 cells that have been transfected with GFP-labeled G59S p150^{Glued} and immunolabeled with an antibody to GFP. Inclusions (i) and nuclei (n) are labeled. Bars, 500 nm. Inset, immunohistochemistry for DIC was performed on sections from the medulla of an affected patient. Bar, 10 μ m. (C) High-magnification electron micrograph of a COS7 cell that has been transfected with GFP-labeled G59S p150^{Glued} and fixed with glutaraldehyde. No membrane surrounds the inclusion; the visible membrane is a nuclear envelope. Arrows indicate mitochondria surrounding and within G59S p150^{Glued} protein inclusions. Bar, 500 nm. (D and E) COS7 cells transfected with GFP-tagged wild-type (D) or G59S (E) p150^{Glued} and fixed and stained using antibodies for p150^{Glued} and Hsp60. Bar, 10 μ m. (F) Quantification of area of cells containing mitochondria in arbitrary units, \pm SEM (*, $P < 0.05$). Wild type, $n = 8$; G59S, $n = 12$.



As shown in Fig. 1 C, G59S p150^{Glued} was cytoplasmically dispersed in COS7 cells 24–48 h after transfection, whereas wild-type p150^{Glued} decorated microtubules. At longer time points, however, we noted a centripetal localization of the proteins. Wild-type p150^{Glued} became preferentially localized along microtubules in the perinuclear region (Fig. 6 C). In contrast, G59S p150^{Glued} localized to inclusions surrounding the nucleus, which may correspond to the aggresomes of misfolded protein described by Johnston et al. (2002). These structures were also observed in very highly expressing cells at earlier time points, but their frequency increased with time after transfection (Fig. S3, available at <http://www.jcb.org/cgi/content/full/jcb.200511068/DC1>). In some MN1 cells transfected with GFP-tagged G59S p150^{Glued}, single or multiple inclusions were evident most often in the cell body (Fig. 6 D) and rarely in neurites. They were similar in appearance to those observed in motor neurons from the brainstem of an affected patient (Puls et al., 2005), and their frequency increased with time after transfection (Fig. S3). Inclusions stained positive for dynein intermediate chain (DIC), the Golgi marker GM130, and the 20S proteasome but not kinesin heavy chain, microtubules, neurofilaments, vimentin, microtubule-associated protein 2, Cu/Zn superoxide dismutase (SOD1), and survival of motor neurons,

(unpublished data). Thus, in both neuronal and nonneuronal cells, mutation of the glycine 59 appears to decrease microtubule binding by the p150^{Glued} CAP-Gly domain and leads to aggregation and inclusion formation by the mutant protein.

Inclusions of mutant protein are granular and associated with mitochondria

To look at the ultrastructure of the inclusions, transfected COS7 cells and MN1 cells were observed by EM. MN1 cells transfected with GFP-tagged full-length G59S p150^{Glued} and labeled with immunogold showed granular, nonfibrillar inclusions of mutant protein (Fig. 7, A and B). Analysis of nonimmunogold-labeled, glutaraldehyde-fixed COS7 cells demonstrated that the inclusions were not membrane bound (Fig. 7 C). These micrographs show inclusions that look remarkably like the dynein- and dynactin-containing inclusions seen in patient neurons by immunohistochemistry (Puls et al., 2005).

In these ultrastructural studies, mitochondria frequently surrounded or were contained within the G59S p150^{Glued} inclusions (Fig. 7 C). To examine the possibility that mitochondria localization was altered by the inclusions, COS7 cells were transfected with wild-type or G59S p150^{Glued} and stained with an antibody to mitochondrial chaperone Hsp60. Mitochondria

were partially relocated in the area of the aggregates (Fig. 7, D and E). Quantification of the cross-sectional area of the cells that contained mitochondria demonstrated that mitochondria in cells transfected with G59S p150^{Glued} were less widely distributed than in cells transfected with wild-type protein (Fig. 7 F). It may be that mitochondria cannot be transported to the cell periphery because of aberrant interaction with the aggregated G59S p150^{Glued}. Alternatively, it is possible that loss of dynein/dynactin transport causes mitochondrial mislocalization, as expression of dynamitin has also been shown to cause an inward collapse of the mitochondrial array (Varadi et al., 2004).

Expression of G59S p150^{Glued} induces death in neuronal cells

The expression of the G59S polypeptide led to an increase in cell death in MN1 cells, as determined by propidium iodide (PI) exclusion. Cells were transfected with GFP-tagged wild-type p150^{Glued}, G59S p150^{Glued}, or GFP alone. The MN1 cells transfected with G59S p150^{Glued} demonstrated a significantly higher percentage of cell death than cells transfected with wild-type p150^{Glued} or GFP alone (Fig. 8 A). Furthermore, the percentage of cell death increased with time after transfection, corresponding to an increase in the percentage of cells containing inclusions visible by immunofluorescence (Fig. S3). Embryonic rat motor neurons expressing G59S p150^{Glued} also demonstrated an increase in cell death compared with motor neurons expressing exogenous wild-type p150^{Glued} in a time-dependent manner (Kalb, R.G., personal communication). Neuronal cells may be uniquely sensitive to the G59S polypeptide, as the expression of G59S p150^{Glued} does not increase cell death in COS7 cells (Fig. 8 A).

Overexpression of Hsp70 inhibits formation of G59S p150^{Glued} aggregates and prevents cell death

Overexpression of the chaperone Hsp70 has been reported to suppress protein aggregate formation and prevent cell death in several protein misfolding disease models (Barral et al., 2004). 56 ± 6% of COS7 cells expressing the G59S p150^{Glued} protein for 2 d contained visible inclusions (Fig. 8, B and E). However, cells expressing both Hsp70 and G59S p150^{Glued} exhibited a disperse localization of both exogenous proteins and only 17 ± 4% of transfected cells contained visible inclusions (Fig. 8, C and E). Hsp70 containing the T13G mutation cannot undergo the conformational change necessary for chaperone activity (Sousa and McKay, 1998). In cells cotransfected with G59S p150^{Glued} and T13G Hsp70, the proportion of cells containing inclusions was not significantly different from that of cells transfected with G59S p150^{Glued} alone (Fig. 8, D and E). A Western blot of the cell protein lysates showed that levels of G59S p150^{Glued} were decreased when wild-type, but not T13G, Hsp70 was co-expressed (Fig. 8 F). The chaperone function of Hsp70 may aid proper folding of G59S p150^{Glued}, thereby avoiding the formation of inclusions and allowing effective degradation of the mutant protein by the ubiquitin–proteasome pathway.

Transfection of G59S p150^{Glued} into MN1 cells led to an increase in cell death compared with cells transfected with wild-type p150^{Glued} (Fig. 8 A). However, coexpression of G59S

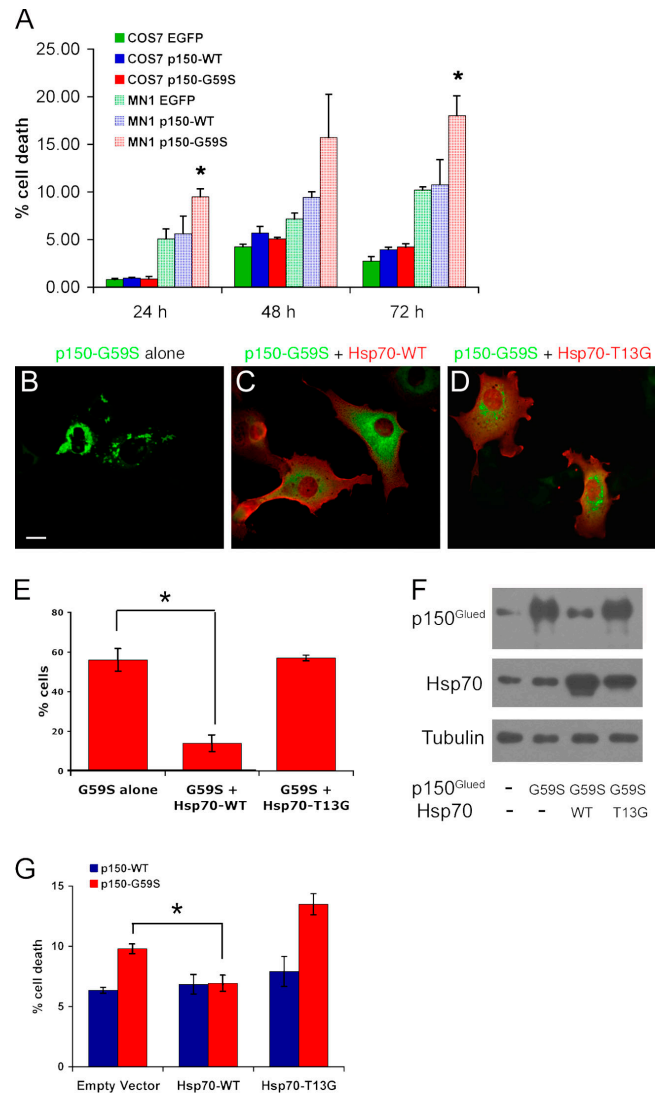


Figure 8. Overexpression of Hsp70 decreases both aggregation of G59S p150^{Glued} and MN1 cell death. (A) Quantitation of cell death after transfection with wild-type (WT) or G59S p150^{Glued} or EGFP alone, as determined by PI exclusion. Values represent mean percentage of cell death in three sets of transfections, ± SEM (*, *P* < 0.05). *n* = 3. (B–D) Representative images of cells transfected with G59S p150^{Glued} alone (B), G59S p150^{Glued} and wild-type Hsp70 (C), or G59S p150^{Glued} and T13G Hsp70 (D). Cells were stained with antibodies for p150^{Glued} (green) and the hemagglutinin tag on the Hsp70 constructs (red). Bar, 10 μm. (E) Quantitation of the percentage of COS7 cells containing aggregates, ± SD (*, *P* < 0.05). *n* = 2. (F) Expression levels of p150^{Glued} and Hsp70 in lysates from cells that have been mock-transfected, transfected with G59S alone, and transfected with wild-type or T13G Hsp70. Tubulin was used as a loading control. (G) Quantitation of mean percentage of cell death in MN1 cells 48 h after transfection with wild-type and G59S p150^{Glued} and wild-type and T13G Hsp70 or empty vector, ± SEM (*, *P* < 0.05). Cotransfection of G59S p150^{Glued} and wild-type Hsp70 protects MN1 cells from death, but cotransfection of G59S p150^{Glued} with T13G Hsp70 or empty vector does not. *n* = 3.

p150^{Glued} and wild-type Hsp70 reduced the percentage of MN1 cell death to levels similar to those of cells transfected with wild-type p150^{Glued} (Fig. 8 G). This protection was not observed when MN1 cells were cotransfected with G59S p150^{Glued} and either empty vector or T13G Hsp70 (Fig. 8 G). These data demonstrate that expression of active Hsp70 reduces the amount of

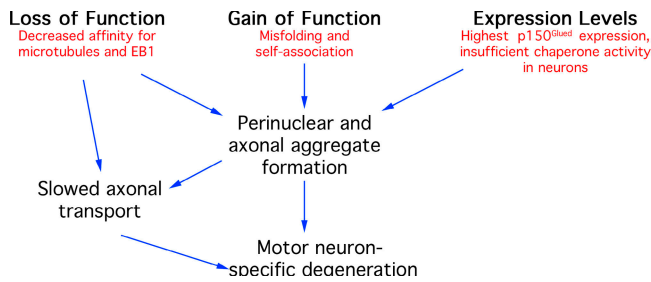


Figure 9. **Proposed mechanism of G59S p150^{Glued}-mediated motor neuron toxicity.** G59S p150^{Glued} expression leads to motor neuron toxicity through three intersecting pathways that lead to cell death. The mutation causes impaired microtubule and EB1 binding, which leads to disrupted dynein/dynactin-based transport. In addition, the mutation causes misfolding of the CAP-Gly domain, which leads to aberrant self-association. The large proportion of unbound p150^{Glued}, along with the high expression levels of p150^{Glued} in neurons, leads to a high cytosolic concentration of misfolded mutant protein resulting in aggregates specifically in neurons. This gain of function may induce further impairment in axonal transport, either by physical blockage of the axon or by sequestration of dynein and dynactin, leading to motor neuron-specific degeneration.

G59S p150^{Glued} aggregates, decreases the amount of p150^{Glued} expressed, and protects MN1 cells from the toxicity associated with expression of the mutant p150^{Glued}.

Discussion

A key question in the analysis of many neurodegenerative diseases is the cell-type specificity observed: why would a mutation in a ubiquitously expressed protein preferentially affect a single cell type? This question is particularly critical in the study of motor neuron diseases, such as Amyotrophic Lateral Sclerosis, in which multiple mutations in a ubiquitously expressed protein, SOD1, result in motor neuron-specific degeneration and cell death. Several mechanisms have been proposed, including neuron-specific aggregation and defects in axonal transport (for review see Bruijn et al., 2004).

We focus on the cellular effects of a point mutation in the p150^{Glued} subunit of dynactin. Dynactin is ubiquitously expressed in vertebrates, interacting with cytoplasmic dynein to serve as the major motor for microtubule minus end-directed transport in the cell. The dynein-dynactin complex is required for a range of cellular functions, including mitotic spindle assembly, ER-to-Golgi trafficking, and endosome and lysosome motility. Although complete loss of dynactin function is therefore likely to affect all cell types, patients expressing the G59S mutation in the p150^{Glued} subunit of dynactin develop an autosomal-dominant, slowly progressive degeneration specific to motor neurons (Puls et al., 2003).

The G59S missense mutation results in a subtle impairment of dynactin function. A subtle loss of function in a protein required for retrograde axonal transport may be sufficient to induce a slow degeneration of motor neurons. Mice with a targeted disruption in dynactin function or with point mutations in cytoplasmic dynein heavy chain exhibit a slowly progressive loss of motor neurons, resulting in muscle atrophy (LaMonte et al., 2002; Hafezparast et al., 2003).

The G59S mutation also results in a toxic gain of function, as the G59S polypeptide is prone to aggregate. Parrini et al. (2005) have shown that evolutionarily conserved glycines inhibit aggregation because of their low propensity to form β structure. The G59S substitution alters a highly conserved glycine residue within the NH₂-terminal CAP-Gly domain of the protein and is predicted to result in steric crowding and misfolding of this domain (Puls et al., 2003).

Comparisons of aggregate formation in both neuronal and nonneuronal cells overexpressing the G59S mutation suggest that motor neurons are uniquely vulnerable to aggregate formation, leading to enhanced cell death. One explanation for this observation is that motor neurons may not express adequate levels of chaperones to cope with the high levels of misfolded protein. Recent studies have shown that motor neurons are not able to up-regulate Hsp70 in response to cellular stress and that they are particularly vulnerable to depletion of Hsp70 (Robinson et al., 2005). Consistent with this mechanism, overexpression of Hsp70 led to decreased aggregations of the G59S polypeptide and decreased cell death.

The mechanism by which aggregate formation leads to cell death remains to be determined. However, EM analysis of the aggregates demonstrates the presence of trapped organelles, including mitochondria. The aggregates may either actively trap organelles or passively disrupt microtubule-based transport via “organelle jams” (for review see Holzbaur, 2004). The sequestration of cytoplasmic dynein in these aggregates, as observed in both transfected cells and patient motor neurons (Puls et al., 2005), would further disrupt axonal transport. This disruption in transport is likely to be most deleterious to motor neurons because of their overall size and extended axons.

Based on our observations, we propose the following model to explain the motor neuron-specific phenotype observed in patients expressing the G59S mutation in dynactin (Fig. 9). The mutation leads to a decreased efficiency in minus end-directed transport. This subtle loss of function does not significantly perturb nonneuronal cells but may be sufficient to affect the overall efficiency of retrograde axonal transport in neurons. However, the mutation also results in a gain of function, as the G59S polypeptide has an enhanced propensity to misfold. Aggregation of the misfolded protein is concentration dependent, and the p150^{Glued} polypeptide is highly expressed in motor neurons (Melloni et al., 1995; unpublished data). Further, motor neurons may be specifically vulnerable to misfolding and aggregation of the G59S polypeptide because of insufficient expression of molecular chaperones. Finally, both the sequestration of active motors and the trapping of organelles by the p150^{Glued} aggregates will further exacerbate the inhibition of axonal transport.

Together, our data provide the foundation for a testable model for the cellular mechanisms leading to the motor neuron-specific degeneration observed in patients expressing the G59S mutation, involving both loss of function and toxic gain of function. We anticipate that these studies will provide further insight into the mechanisms by which a mutation in an essential cellular protein can result in specific degeneration of motor neurons in vivo.

Materials and methods

Microtubule binding

Wild-type and G59S p150^{Glu} were expressed and labeled with [³⁵S]methionine using the TNT T7 Quick system (Promega), clarified by centrifugation at 39,000 g for 30 min, incubated for 30 min at 20°C with increasing concentrations of microtubules polymerized from purified tubulin (Cytoskeleton, Inc.), and stabilized with paclitaxel (Cytoskeleton, Inc.). Microtubule bound and unbound proteins were separated by centrifugation at 39,000 g for 20 min and analyzed by SDS-PAGE and fluorography. Results were quantitated by densitometry using NIH ImageJ. Prism Software (GraphPad) was used to fit the binding data to the one-site ligand binding equation $y = B_{max} \times x / (K_d + x)$.

Affinity chromatography and Western blot

Affinity matrices were prepared by cross-linking recombinant EB1 to activated CH Sepharose 4B (GE Healthcare) beads at 4 mg/ml ligand. In vitro-expressed p150^{Glu} was incubated with the EB1-bound beads for 30 min at room temperature. These mixtures were loaded onto a column and washed extensively with 50 mM Tris and 25 mM KCl, pH 7.4, with 0.1% Triton X-100. Retained proteins were eluted with 2 M NaCl. Fractions were analyzed by SDS-PAGE and Western blot.

Cell culture, transfections, immunocytochemistry, and nocodazole recovery assay

Fibroblast cell lines were derived from forearm punch skin biopsies from two symptomatic patients with the G59S mutation and from an age-matched, unaffected control sibling (Priest, 1997). An additional age-matched control fibroblast line (AG02222) was obtained from the Coriell Cell Repository. Lymphoblast cell lines were derived from blood samples from an affected family member carrying the G59S mutation using standard techniques. Cell lines were established in the Cytogenetics Laboratory at Georgetown University.

Fibroblast cell lines were maintained in Hams F-10 culture media supplemented with 15% fetal bovine serum; lymphoblast cells were maintained in RPMI media with 10% fetal bovine serum. COS7 cells (American Type Culture Collection) were maintained as described previously (Ligon et al., 2003). HeLa-M cells (a gift from A. Peden, Genentech, South San Francisco, CA) were maintained in DME with 10% fetal bovine serum. For immunofluorescence assays, cells were grown to ~75% confluence and then fixed in -20°C methanol and processed for immunocytochemistry. Monoclonal antibodies to tubulin (DM1A from Sigma-Aldrich), hemagglutinin (Sigma-Aldrich), kinesin heavy chain (Chemicon), neurofilament (NE14 from Sigma-Aldrich), vimentin (Sigma-Aldrich), microtubule-associated protein 2 (Sigma-Aldrich), Cu/Zn SOD1 (StressGen Biotechnologies), survival of motor neurons (BD Biosciences), Golgi protein GM130 (BD Biosciences), cytoplasmic DIC (Chemicon), EB1 (BD Biosciences), TGN46 (Serotech), Hsp60 and -70 (StressGen Biotechnologies), and dynactin subunits p150^{Glu} and dynamitin (BD Biosciences) were purchased commercially. Affinity-purified polyclonal antibodies to p150^{Glu}, Arp1, and DIC have been described previously (Holleran et al., 1996; Tokito et al., 1996; Ligon et al., 2001). Immunostaining was visualized with Alexa 350-, 488-, and 594-conjugated secondary antibodies (Invitrogen). Images were acquired on a microscope (DMIRBE; Leica) with a 63× or 100× Plan Apo objective using OpenLab software (Improvision) and a charged-coupled device camera (Orca ER; Hamamatsu).

MN1 cells were maintained as described previously (Brooks et al., 1998) and fixed in 4% paraformaldehyde at room temperature for 10 min, permeabilized with 0.1% Triton X-100 in PBS for 10 min, and incubated with monoclonal antibodies to α -tubulin (clone 2.1 from Sigma-Aldrich) followed by Texas red-conjugated secondary antibodies (Jackson Immuno-Research Laboratories). Deconvoluted images were acquired with a microscope (Olympus) using DeltaVision software (Applied Precision) on a Silicon Graphics workstation.

Transient transfection assays were performed using Fugene (Roche) and plasmids encoding either wild-type or G59S full-length human p150^{Glu} or truncated constructs of the wild-type and G59S polypeptide spanning residues 1–333, both fused to GFP and untagged. Hemagglutinin-tagged Hsp70 constructs were a gift from Y. Argon (University of Pennsylvania, Philadelphia, PA).

For nocodazole recovery assays, patient and control fibroblasts were treated with nocodazole at 5 μ g/ml for 1 h and then allowed to recover for 0, 30, or 60 min or 24 h in conditioned culture media at 37°C in 5% CO₂ before fixation.

Microtubule plus-end dynamics assay

Live cell time-lapse recordings were performed on transiently transfected COS7 cells expressing either full-length wild-type or G59S p150^{Glu} or NH₂-terminal residues 1–333 of wild-type or G59S p150^{Glu}, all fused to GFP. Cells on glass coverslips were sealed in an imaging chamber (FCS2; Biophtechs) and maintained at 37°C in culture media. Sequential time-lapse fluorescent images were acquired at 12-s intervals.

RNA interference

HeLa-M cells were transfected using Oligofectamine (Invitrogen) with 100 nM of a mixture of four RNA duplexes targeting different regions of human DCTN1 (SMARTpool siRNA reagent [Dharmacon]; available from GenBank/EMBL/DBJ under accession no. NM_004082): 5'-gaagacgagagacaguu-3', 5'-cgagcucacucacugacuu-3', 5'-caugagcgcuccuug-gauu-3', and 5'-ggagcgcuguaucgaa-3'. Cells were transfected after 72 h and processed for immunocytochemistry or resuspended in denaturing sample buffer and processed for Western blot analysis.

RNA extraction and quantitative RT-PCR

RNA was extracted from cells using TRIzol (Invitrogen) and purified with the RNAeasy clean-up kit according to the manufacturer's protocol (QIAGEN), and cDNAs were generated using the High Capacity cDNA Achieve kit (Applied Biosystems). Quantitative PCR reactions were run in triplicate using the ABI Prism 7900 sequence detection system (Applied Biosystems). A forward primer (5'-gaaggcctgcatctttgtg-3'), a reverse primer (5'-gaagcagaagaatcagggtctct-3'), and a fluorescent probe (5'-FAM-ccagtccagatccag-BHQ1-3') were designed to amplify p150^{Glu} transcripts. Endogenous controls were simultaneously amplified using commercially available primers (Applied Biosystems). The reactions were performed in triplicate and averaged, and p150^{Glu} Ct values (cycle number when signal reaches a threshold above background) were corrected for endogenous control Ct values using the $\Delta\Delta$ Ct method per the Applied Biosystems User Bulletin 2.

Sucrose density gradient centrifugation

Cells from 3–6 flasks of patient fibroblasts and 3–6 flasks of control fibroblasts were washed in PBS, harvested, and homogenized in 20 mM Tris-HCl, pH 7.4, 2 mM EGTA, and 1 mM EDTA with protease inhibitors (leupeptin, pepstatin A, N-p-tosyl-L-arginine methyl ester, and PMSF). Triton X-100 was added to 0.4%, and the homogenate was clarified by low-speed centrifugation. The resulting supernatant fraction was layered over a 5–25% linear sucrose density gradient and centrifuged at 126,000 g for 16 h. The gradients were eluted in 0.5-ml fractions, which were resolved by SDS-PAGE, and analyzed by Western blot.

Aggregation assays

For aggregation assays, His- and T7-tagged constructs of wild-type and G59S p150^{Glu} were coexpressed in vitro and incubated for 2 h at 30°C. The reactions were then incubated sequentially with protein A beads to preclear the extracts, followed by protein A beads with bound monoclonal antibody to T7 (Novagen). After a 1-h incubation with antibody bound beads, the beads were isolated by centrifugation; washed four times with 50 mM Tris, pH 7.3, 50 mM NaCl, and 0.1% Triton X-100; and eluted by boiling in denaturing gel sample buffer. The immunoprecipitates were analyzed by Western blot probed with antibodies to the His and T7 tags.

Cell death assays

A FACS-based survival assay was used to measure cell death (Taylor et al., 2003). MN1 or COS7 cells were transfected with pEGFP wild-type and G59S p150 constructs in 6-well plates. Each transfection condition was performed in triplicate. After 24, 48, or 72 h, cells were harvested with trypsin, gently pelleted with centrifugation, and resuspended in 1 ml of PBS. Cells were stained with 2 μ g/ml PI (Sigma-Aldrich) and gently vortexed. For each sample, 50,000 nongated events were acquired using a FACSCalibur instrument (BD Biosciences) and Cell Quest software (Becton Dickinson). GFP fluorescence was collected in the FL-1 channel, and PI fluorescence was collected in the FL-3 channel in dot and density blot formats. Results were expressed as a percentage of PI-positive cells (cell death) divided by the total number of GFP-positive cells (transfected cells).

EM

MN1 and COS7 cells were plated on permanox chambered slides (Lab-Tek; Nunc) and transfected with pEGFP wild-type and G59S p150 constructs or wild-type and G59S p150^{Glu} (untagged) constructs. 48 h after transfection, one set of cells (for immunogold labeling) was fixed with 4% paraformaldehyde in PBS for 1 h and another set was fixed in

4% glutaraldehyde in cacodylate buffer. Paraformaldehyde-fixed cells were washed three times with PBS and then blocked and permeabilized with 0.1% saponin for 1 h. The p150^{Glued}-GFP-transfected cells were then incubated with mouse polyclonal GFP antibody (Invitrogen), and p150^{Glued}-transfected cells were incubated in dynactin polyclonal antibody (UP235) followed by anti-mouse or anti-rabbit Nanogold (Nanoprobes). Slides were subjected to staining and silver enhancement as described previously (Tanner et al., 1996). After dehydration, embedding, and sectioning, samples were examined with an electron microscope (1200EX; JEOL).

Online supplemental material

Fig. S1 shows sequential and mixed microtubule binding of G59S p150^{Glued}. Fig. S2 shows that the localization of p150^{Glued} and the formation of spindles are normal in cells heterozygous for the G59S mutation in p150^{Glued}. Fig. S3 shows that the percentage of cells containing G59S p150^{Glued} inclusions increases with time after transfection. Video 1 shows microtubule plus-end tracking of GFP-labeled wild-type p150^{Glued} in transfected COS7 cells. Video 2 demonstrates a loss of microtubule tip localization and plus-end tracking of GFP-labeled G59S p150^{Glued} in transfected COS7 cells. Online supplemental material is available at <http://www.jcb.org/cgi/content/full/jcb.200511068/DC1>.

We gratefully acknowledge the members of the affected family for their willing participation. We thank Susan Cheng and Virginia Crocker in the National Institute of Neurological Disorders and Stroke EM Core Facility, Barbara Crain in the Johns Hopkins Department of Pathology, and Anish Patel and Maura Strauman for technical contributions.

This work was supported by National Institutes of Health grant GM48661 (to E.L.F. Holzbaur), National Institutes of Health/National Institute on Aging training grant T32 AG00255 (to J.R. Levy), National Institute of Neurological Disorders and Stroke Career Transition award K22-NS0048199-01 (to C.J. Sumner), funds from the Intramural Research Program of the National Institutes of Health (to C.J. Sumner, S. Ranganathan, G. G. Harmison, I. Puls, and K.H. Fischbeck), and a grant from the Amyotrophic Lateral Sclerosis Association (to E.L.F. Holzbaur).

Submitted: 17 November 2005

Accepted: 31 January 2006

References

Barral, J.M., S.A. Broadley, G. Schaffar, and F.U. Hartl. 2004. Roles of molecular chaperones in protein misfolding diseases. *Semin. Cell Dev. Biol.* 15:17–29.

Brooks, B.P., D.E. Merry, H.L. Paulson, A.P. Lieberman, D.L. Kolson, and K.H. Fischbeck. 1998. A cell culture model for androgen effects in motor neurons. *J. Neurochem.* 70:1054–1060.

Brujin, L.I., T.M. Miller, and D.W. Cleveland. 2004. Unraveling the mechanisms involved in motor neuron degeneration in ALS. *Annu. Rev. Neurosci.* 27:723–749.

Burkhardt, J.K., C.J. Echeverri, T. Nilsson, and R.B. Vallee. 1997. Overexpression of the dynamitin (p50) subunit of the dynactin complex disrupts dynein-dependent maintenance of membrane organelle distribution. *J. Cell Biol.* 139:469–484.

Carson, J.H., H. Cui, and E. Barbaresi. 2001. The balance of power in RNA trafficking. *Curr. Opin. Neurobiol.* 11:558–563.

Corthesy-Theulaz, I., A. Pauloin, and S. Rfeffer. 1992. Cytoplasmic dynein participates in the centrosomal localization of the Golgi complex. *J. Cell Biol.* 118:1333–1345.

Dohner, K., A. Wolfstein, U. Prank, C. Echeverri, D. Dujardin, R. Vallee, and B. Sodeik. 2002. Function of dynein and dynactin in herpes simplex virus capsid transport. *Mol. Biol. Cell.* 13:2795–2809.

Dujardin, D.L., L.E. Barnhart, S.A. Stehman, E.R. Gomes, G.G. Gundersen, and R.B. Vallee. 2003. A role for cytoplasmic dynein and LIS1 in directed cell movement. *J. Cell Biol.* 163:1205–1211.

Echeverri, C.J., B.M. Paschal, K.T. Vaughan, and R.B. Vallee. 1996. Molecular characterization of the 50-kD subunit of dynactin reveals function for the complex in chromosome alignment and spindle organization during mitosis. *J. Cell Biol.* 132:617–633.

Gepner, J., M. Li, S. Ludmann, C. Kortas, K. Boylan, S.J. Iyadurai, M. McGrail, and T.S. Hays. 1996. Cytoplasmic dynein function is essential in *Drosophila melanogaster*. *Genetics.* 142:865–878.

Hafezparast, M., R. Klocke, C. Ruhrberg, A. Marquardt, A. Ahmad-Annuar, S. Bowen, G. Lalli, A.S. Witherden, H. Hummerich, S. Nicholson, et al.

2003. Mutations in dynein link motor neuron degeneration to defects in retrograde transport. *Science.* 300:808–812.

Harada, A., Y. Takei, Y. Kanai, Y. Tanaka, S. Nonaka, and N. Hirokawa. 1998. Golgi vesiculation and lysosome dispersion in cells lacking cytoplasmic dynein. *J. Cell Biol.* 141:51–59.

Harte, P.J., and D.R. Kankel. 1983. Analysis of visual system development in *Drosophila melanogaster*: mutations at the Glued locus. *Dev. Biol.* 99:88–102.

Hayashi, I., A. Wilde, T.K. Mal, and M. Ikura. 2005. Structural basis for the activation of microtubule assembly by the EB1 and p150^{Glued} complex. *Mol. Cell.* 19:449–460.

Holleran, E.A., M.K. Tokito, S. Karki, and E.L. Holzbaur. 1996. Centractin (ARP1) associates with spectrin revealing a potential mechanism to link dynactin to intracellular organelles. *J. Cell Biol.* 135:1815–1829.

Holzbaur, E.L. 2004. Motor neurons rely on motor proteins. *Trends Cell Biol.* 14:233–240.

Hoogenraad, C.C., A. Akhmanova, F. Grosveld, C.I. De Zeeuw, and N. Galjart. 2000. Functional analysis of CLIP-115 and its binding to microtubules. *J. Cell Sci.* 113:2285–2297.

Johnston, J.A., M.E. Illing, and R.R. Kopito. 2002. Cytoplasmic dynein/dynactin mediates the assembly of aggresomes. *Cell Motil. Cytoskeleton.* 53:26–38.

LaMonte, B.H., K.E. Wallace, B.A. Holloway, S.S. Shelly, J. Ascano, M. Tokito, T. Van Winkle, D.S. Howland, and E.L. Holzbaur. 2002. Disruption of dynein/dynactin inhibits axonal transport in motor neurons causing late-onset progressive degeneration. *Neuron.* 34:715–727.

Ligon, L.A., S. Karki, M. Tokito, and E.L. Holzbaur. 2001. Dynein binds to beta-catenin and may tether microtubules at adherens junctions. *Nat. Cell Biol.* 3:913–917.

Ligon, L.A., S.S. Shelly, M. Tokito, and E.L. Holzbaur. 2003. The microtubule plus-end proteins EB1 and dynactin have differential effects on microtubule polymerization. *Mol. Biol. Cell.* 14:1405–1417.

Melloni, R.H., Jr., M.K. Tokito, and E.L. Holzbaur. 1995. Expression of the p150^{Glued} component of the dynactin complex in developing and adult rat brain. *J. Comp. Neurol.* 357:15–24.

Merry, D.E., Y. Kobayashi, C.K. Bailey, A.A. Taye, and K.H. Fischbeck. 1998. Cleavage, aggregation and toxicity of the expanded androgen receptor in spinal and bulbar muscular atrophy. *Hum. Mol. Genet.* 7:693–701.

Parrini, C., N. Taddei, M. Ramazzotti, D. Degl'Innocenti, G. Ramponi, C.M. Dobson, and F. Chiti. 2005. Glycine residues appear to be evolutionarily conserved for their ability to inhibit aggregation. *Structure.* 13:1143–1151.

Priest, J.H. 1997. General cell culture principles and fibroblast culture. In *The AGT Cytogenetics Laboratory Manual*. M.J. Barch, T. Knutsen, and J.L. Spurbeck, editors. Lippincott-Raven, Philadelphia. 173–197.

Puls, I., C. Jonnakuty, B.H. LaMonte, E.L. Holzbaur, M. Tokito, E. Mann, M.K. Floeter, K. Bidus, D. Drayna, S.J. Oh, et al. 2003. Mutant dynactin in motor neuron disease. *Nat. Genet.* 33:455–456.

Puls, I., S.J. Oh, C.J. Sumner, K.E. Wallace, M.K. Floeter, E.A. Mann, W.R. Kennedy, G. Wendelschafer-Crabb, A. Vortmeyer, R. Powers, et al. 2005. Distal spinal and bulbar muscular atrophy caused by dynactin mutation. *Ann. Neurol.* 57:687–694.

Robinson, M.B., J.L. Tidwell, T. Gould, A.R. Taylor, J.M. Newbern, J. Graves, M. Tytell, and C.E. Milligan. 2005. Extracellular heat shock protein 70: a critical component for motoneuron survival. *J. Neurosci.* 25:9735–9745.

Salazar-Grueso, E.F., S. Kim, and H. Kim. 1991. Embryonic mouse spinal cord motor neuron hybrid cells. *Neuroreport.* 2:505–508.

Schroer, T.A. 2004. Dynactin. *Annu. Rev. Cell Dev. Biol.* 20:759–779.

Sousa, M.C., and D.B. McKay. 1998. The hydroxyl of threonine 13 of the bovine 70-kDa heat shock cognate protein is essential for transducing the ATP-induced conformational change. *Biochemistry.* 37:15392–15399.

Tanner, V.A., T. Ploug, and J.H. Tao-Cheng. 1996. Subcellular localization of SV2 and other secretory vesicle components in PC12 cells by an efficient method of preembedding EM immunocytochemistry for cell cultures. *J. Histochem. Cytochem.* 44:1481–1488.

Taylor, J.P., F. Tanaka, J. Robitschek, C.M. Sandoval, A. Taye, S. Markovic-Plese, and K.H. Fischbeck. 2003. Aggresomes protect cells by enhancing the degradation of toxic polyglutamine-containing protein. *Hum. Mol. Genet.* 12:749–757.

Tokito, M.K., D.S. Howland, V.M. Lee, and E.L. Holzbaur. 1996. Functionally distinct isoforms of dynactin are expressed in human neurons. *Mol. Biol. Cell.* 7:1167–1180.

Varadi, A., L.I. Johnson-Cadwell, V. Cirulli, Y. Yoon, V.J. Allan, and G.A. Rutter. 2004. Cytoplasmic dynein regulates the subcellular distribution

- of mitochondria by controlling the recruitment of the fission factor dynamin-related protein-1. *J. Cell Sci.* 117:4389–4400.
- Vaughan, K.T., and R.B. Vallee. 1995. Cytoplasmic dynein binds dynactin through a direct interaction between the intermediate chains and p150^{Glued}. *J. Cell Biol.* 131:1507–1516.
- Vaughan, K.T., S.H. Tynan, N.E. Faulkner, C.J. Echeverri, and R.B. Vallee. 1999. Colocalization of cytoplasmic dynein with dynactin and CLIP-170 at microtubule distal ends. *J. Cell Sci.* 112:1437–1447.
- Waterman-Storer, C.M., S. Karki, and E.L. Holzbaur. 1995. The p150^{Glued} component of the dynactin complex binds to both microtubules and the actin-related protein capping protein (Arp-1). *Proc. Natl. Acad. Sci. USA.* 92:1634–1638.